Science and Technology of Advanced Materials

ISSN: (Print) (Online) Journal homepage: www.tandfonline.com/journals/tsta20

High performance {Nb_5TaX_{12}}@PVP (X = Cl, Br) cluster-based nanocomposites coatings for solar glazing applications

Clément Lebastard, Maxence Wilmet, Stéphane Cordier, Clothilde Comby-Zerbino, Luke MacAleese, Philippe Dugourd, Naoki Ohashi, Tetsuo Uchikoshi & Fabien Grasset

To cite this article: Clément Lebastard, Maxence Wilmet, Stéphane Cordier, Clothilde Comby-Zerbino, Luke MacAleese, Philippe Dugourd, Naoki Ohashi, Tetsuo Uchikoshi & Fabien Grasset (2022) High performance {Nb_5TaX_{12}}@PVP (X = Cl, Br) cluster-based nanocomposites coatings for solar glazing applications, Science and Technology of Advanced Materials, 23:1, 446-456, DOI: 10.1080/14686996.2022.2105659

To link to this article: https://doi.org/10.1080/14686996.2022.2105659

SCIENCE AND TECHNOLOGY OF ADVANCED MATERIALS
2022, VOL. 23, NO. 1, 446–456
https://doi.org/10.1080/14686996.2022.2105659

Taylor & Francis
Taylor & Francis Group

FOCUS ISSUE ARTICLE

High performance $\{Nb_5TaX_{12}\}$@PVP (X = Cl, Br) cluster-based nanocomposites coatings for solar glazing applications

Clément Lebastard[a,b], Maxence Wilmet[a,b,c], Stéphane Cordier[a], Clothilde Comby-Zerbino[d], Luke MacAleese[d], Philippe Dugourd[d], Naoki Ohashi[b,e], Tetsuo Uchikoshi[b,e] and Fabien Grasset[a,b]

[a]Université Rennes, CNRS, ISCR, UMR6226, F-35000 Rennes, France;
[b]CNRS-Saint Gobain-NIMS, IRL3629, Laboratory for Innovative Key Materials and Structures (LINK), National Institute for Materials Science (NIMS), Tsukuba, Japan;
[c]Saint Gobain Research Paris, Aubervilliers, France;
[d]Univ Lyon, Université Claude Bernard Lyon 1, CNRS, Institut Lumière Matière, F-69622 Lyon, France;
[e]Research Center for Functional Materials, National Institute for Materials Science (NIMS), Tsukuba, Japan

ABSTRACT

The development of highly ultraviolet (UV) and near-infrared (NIR) absorbent transparent coatings is an important enabling technology and area of research for environmental sustainability and energy conservation. Different amounts of $K_4[\{Nb_5TaX^i_{12}\}X^a_6]$ cluster compounds (X = Cl, Br) dispersed into polyvinylpyrrolidone matrices were prepared by a simple, nontoxic and low-cost wet chemical method. The resulting solutions were used to fabricate visibly transparent, highly UV and NIR absorbent coatings by drop casting. The properties of the solution and films were investigated by complementary techniques (optical absorption, electrospray ionization mass spectrometry and Raman spectroscopy). The UV and NIR absorption of such samples strongly depended on the concentration, dispersion and oxidation state of the $[\{Nb_5TaX^i_{12}\}X^a_6]$ nanocluster-based units. By varying and controlling these parameters, a remarkable improvement of the figures of merit T_L/T_E and S_{NIR} for solar-glazing applications was achieved compared to the previous results on nanocomposite coatings based on metal atom clusters.

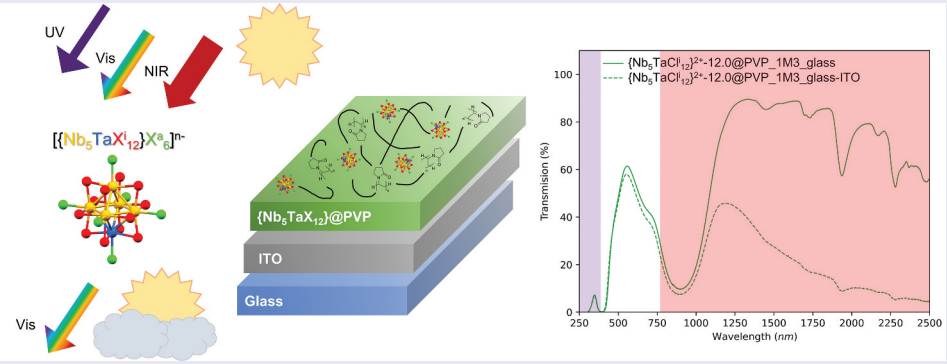

ARTICLE HISTORY
Received 27 May 2022
Revised 7 July 2022
Accepted 19 July 2022

KEYWORDS
Octahedral metal clusters; thin films; nanocomposites; NIR blocker; solar glazing; nanoarchitectonic

I. Introduction

Buildings account for around 40% of global energy consumption [1,2], with more than half of the annual energy consumption of a standard building used in cooling and/or heating systems to maintain their temperature to the range of comfort for their occupants [3]. Through the development of new, environmentally friendly energy saving materials, significant potential for energy savings exists [2]. Approximately 50–55% of incoming solar energy consists of radiation located in the near-infrared (NIR) region of the spectrum, with a majority between 760 and 1100 nm, which are responsible for heat generation (Figure 1) [4,5]. Hence, the use of NIR blockers for smart windows to improve the thermal insulation of buildings and cars is a promising method to reduce overall energy consumption.

Two main approaches for the development of NIR blockers exist, with materials developed either for reflection or absorption of NIR radiations [6]. Currently, some commercialized materials are obtained by vacuum deposition methods, which are quite expensive, limiting their development [7]. New alternatives are turning to the production of absorbing layers deposited by solution deposition processes, with some developed materials summarized in Table 1.

CONTACT Clément Lebastard LEBASTARD.ClementHugo@nims.go.jp; Fabien Grasset fabien.grasset@univ-rennes1.fr Université Rennes, CNRS, ISCR, UMR6226, 263 Avenue du Général Leclerc, F-35000 Rennes, France
Supplemental data for this article can be accessed online at https://doi.org/10.1080/14686996.2022.2105659

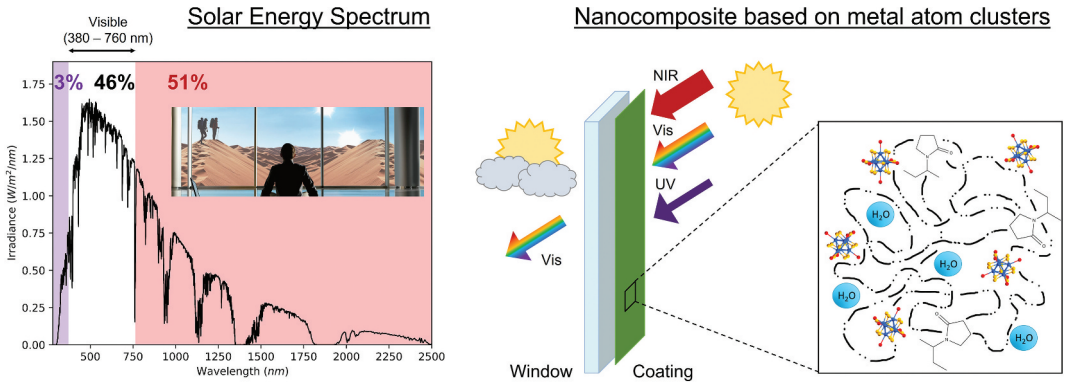

Figure 1. UV-Vis-NIR solar energy spectrum (left) and sketch of the nanocomposite based on metal atom clusters $[\{Nb_5TaX^i_{12}\}X^a_6]^{4-}$ (right).

Table 1. Examples of FOM T_L, T_L and the ratio T_L/T_E (with T_L > 50%). *deposited on polyethylene terephthalate; $deposited on ITO coated glass (noted ITO@glass).

Active species/ Matrix	Ref.	T_L (%)		T_E (%)		T_L/T_E	
LaB_6/PVB	9	81.7		68.3		1.20	
		72.6		50.5		1.44	
		67.8		43.3		1.57	
		62.4		36.6		1.71	
		57.5		31.4		1.83	
Silver nanoprisms	14	92.7		92.9		1.0	
		90.9		89.9		1.01	
		89.5		89.3		1.0	
		81.6		83.0		0.98	
		58.6		60.1		0.98	
		57.5		61.9		0.93	
VO_2 (T=20°C, *T=90°C*)	18	59.2	*61.1*	62.1	*55.7*	0.95	*1.09*
ITO	24	93.0		91.0		1.02	
	36	91.0		78.0		1.24	
	9	87.6		76.6		1.15	
		85.8		59.6		1.44	
AZO	24	85.0		82.0		1.02	
		82.0		62.0		1.32	
$(NH_4)_xWO_3$/PVP*	27	62.1		47.0		1.32	
		61.6		44.4		1.39	
		67.6		45.9		1.47	
Sb doped SnO_2	28	93.9		78.7		1.19	
		92.3		71.9		1.28	
		92.8		70.0		1.33	
		92.0		68.1		1.35	
		90.8		62.0		1.46	
$Cs_{0.32}WO_3$/PMMA	31	85.8		68.8		1.25	
		70.0		43.4		1.74	
		61.8		36.5		1.69	
$\{Ta_6X^i_{12}\}$/PVP$	35	69.9		55.3		1.26	
	36	54.1		46.5		1.16	
		50.6		41.8		1.21	
		62.7		50.0		1.25	
$\{Nb_6X^i_{12}\}$/PMMA$	38	74.1		62.2		1.19	
$\{Nb_6X^i_{12}\}$/PVP	40	62.2		48.3		1.29	
ITO@$\{Nb_6X^i_{12}\}$ @$SiO_2$$	39	61.8		55.6		1.11	
$\{Mo_6X^i_8\}$/PMMA$	38	71.1		57.5		1.24	
$\{Nb_5TaCl^i_{12}\}$/PVP	**This**	**54.1**		**40.7**		**1.33**	
$\{Nb_5TaBr^i_{12}\}$/PVP	**work**	**52.7**		**40.4**		**1.30**	
$\{Nb_5TaCl^i_{12}\}$/PVP$		**53**		**30.6**		**1.73**	

PVB= polyvinyl butyral; AZO= aluminum-doped zinc oxide; PVP= polyvinyl-pyrrolidone; PMMA= Poly(methyl methacrylate).

Generally, the method is based on combining active species with high-infrared absorption and/or reflection properties and a matrix (organic, inorganic or hybrid) which can be deposited by a solution process at the surface of the glass. This method usually requires the use of a large number of active species to achieve interesting solar control properties, which that may induce alterations in the properties of the glazing by scattering (e.g. transparency) or necessitate a more complicated incorporation step. The active species must be on the order of nanometers in size in order to reduce scattering of visible light and to ensure relatively simple integration into the matrix. In order to evaluate the efficiency of the coating as an energy-saving material, different figure-of-merit (FOM) values based on International Commission on Illumination (CIE) colorimetric coordinates, T_L (visible transmittance), T_E (solar transmittance), S_{NIR} (NIR shielding), haze and clarity were measured. T_L, T_E and S_{NIR} were obtained using the equations 1, 2 and 3, respectively [5,8].

$$T_L = \frac{\int_{380}^{760} T(\lambda)S(\lambda)Y(\lambda)d\lambda}{\int_{380}^{760} S(\lambda)Y(\lambda)d\lambda}$$

$$T_E = \frac{\int_{300}^{2500} T(\lambda)S(\lambda)\ d\lambda}{\int_{300}^{2500} S(\lambda)\ d\lambda}$$

$$S_{NIR}(\%) = 100 - \frac{\int_{760}^{2500} T(\lambda)S(\lambda)\ d\lambda}{\int_{760}^{2500} S(\lambda)\ d\lambda}$$

T_E is the integrated spectral transmittance of a window weighted by the normalized solar energy distribution spectrum (noted S). S represents the Air Mass 1.5 which is equivalent to the spectrum of solar radiation after passing through 1.5 times the perpendicular atmospheric thickness. T_L is calculated similarly but weighted by the photopic response of the human eye, Y (see the supplementary information (SI) for more details). The T_L value should be higher than 50%, which is the lower limit acceptable for window applications [5,9–11].

Currently, metal nanoparticles [11–16], oxide materials [17–33] and metalloids [5,34] are considered as the most promising inorganic candidates for NIR blockers. Zheng et al. calculated the period of time required before a return on investment of these most popular solar control materials. Apart from the gold nanoparticles,

other inorganic materials appear to be profitable in less than 30 years [19]. Oxides (In_2O_3:SnO_2 (ITO), WO_3, ZnO, VO_2 ...) and rare earth hexaborides are the most cost-effective, achieving a return on investment under 20 years, which is consistent with the products of the current market (10–20 years) [19]. Recently, it has been shown that the use of Ta_6 or Nb_6 based metal atom clusters leads to nanoarchitectonic coating materials with interesting absorption properties [35–41]. For instance, in these studies, the ability to tune the visible and NIR absorption properties of nanocomposite coatings by oxidation of the $\{Ta_6Br_{12}\}^{2+}$ cluster core into $\{Ta_6Br_{12}\}^{3+}$ or $\{Ta_6Br_{12}\}^{4+}$ cluster cores was investigated [35–39]. This oxidation corresponds to a decrease of the valence electron concentration (VEC) per Ta_6 cluster from 16 for $\{Ta_6Br_{12}\}^{2+}$ to 14 for $\{Ta_6Br_{12}\}^{4+}$ [42].

The absorption of NIR radiations is preferred for a controlled material solar absorber, but the absorption of ultraviolet radiation prevents premature degradation of organic compounds (volatile organic compounds for example). This work is interested in the development of optimized functional coatings including inorganic active species based on metal atom cluster compounds absorbing in adjusted UV and NIR ranges, whilst maintaining a satisfactory level of visible transmittance (Figure 1).

The proposed solutions will revolve around coatings for selective glazing that allows a much better insulation. An optimized coating based on $K_4[\{Nb_5TaX^i_{12}\}X^a_6]$ (X = Cl, Br; I = inner ligand; a = apical ligand) cluster-based compounds embedded in a polyvinylpyrrolidone (PVP) matrix on ITO@Glass is presented. By varying the concentration of clusters and their oxidation states, a large variety of colors from yellow to green were obtained. Additionally, in the frame of solar control applications, the best value of T_L/T_E and S_{NIR} for this family of nanocomposites based on metal atom clusters was measured and reported in this work.

II. Experimental procedures

The $K_4[\{Nb_5TaX^i_{12}\}X^a_6]$ (X = Cl, Br) cluster compounds were prepared by solid-state chemistry using an optimized method derived from that of F. W. Koknat et al. [43,44]. The $[\{Nb_5TaCl^i_{12}\}Cl^a_2(H_2O)^a_4]\cdot 4\,H_2O$ aquo-complex was prepared by following the method proposed for $[\{Ta_6Br^i_{12}\}Br^a_2(H_2O)^a_4]\cdot 4\,H_2O$ and $[\{Nb_6Cl^i_{12}\}Cl^a_2(H_2O)^a_4]\cdot 4\,H_2O$ [40,45] (see the SI for more experimental details and Figures S1 and S2 and Tables S1 and S2).

X-ray Powder diffraction (×RPD) patterns were recorded using a Bruker D8 Advance, Billerica, MA, USA two-circle apparatus equipped with a Lynx Eye detector and Cu Kα radiation (λ = 1.54,056 Å) in the θ – 2θ configuration. Data were collected in the 5–80° 2θ range with a step of 0.02° and a speed of 5°·min^{-1}.

The powder images were observed using a field emission scanning electron microscope (FE-SEM, S4800, Hitachi-Technologies Corp., Tokyo, Japan) at an accelerating voltage of 10kV equipped by an energy-dispersive X-ray (EDX) detector. The cross sections of the films were observed using an optical microscope (Keyence VHX-1000E, Osaka, Japan).

Cluster colloids in PVP were prepared at room temperature by first dissolving an appropriate amount of $K_4[\{Nb_5TaX^i_{12}\}X^a_6]$ (X = Cl, Br) cluster compounds in water solutions (Table 2), followed by filtration. Different concentrations and molar masses of PVP (from 5 to 50%$_{wt}$, 10,000 g·mol^{-1}, 40,000 g·mol^{-1}, 1 300 000 g·mol^{-1}) were tested to obtain a compromise between viscosity, thickness and cluster concentration. The best results were obtained for PVP with a molar mass of 1 300 000 g·mol^{-1} at a concentration of 10%$_{wt}$. Then, PVP (M_w = 1,300,000 g·mol^{-1}) was dissolved and maintained under magnetic stirring until homogenization in the resulting cluster solution. Table 2 shows the different compositions of samples. The solutions are stable for a period of several months.

From these colloids, films (noted $\{Nb_5TaX^i_{12}\}$@PVP) were deposited on soda lime glass slides (up to 10 × 15 cm, Figure S3) or ITO@glass (Geomatec Co., Ltd (Yokohama, Japan), 6–8 Ohm sq^{-1}) by drop casting (1 ml of solution is deposited on the substrate), and dried at room temperature for 24 h. All the substrates were washed with acetone and ethanol before their using. In order to test their durability, some films were annealed in air at 50°C, 80°C and 100°C for 18 hours.

Ultraviolet-visible-near-infrared (UV-Vis-NIR) optical absorption was performed with a spectrophotometer (V7770, Jasco, Oklahoma City, OK, USA), in absorbance and transmission modes, in the range 200–2500 nm. Solutions measured were the same concentrations as the colloids listed in Table 2. Films were measured as-prepared. The CIE Colorimetric System (the CIE 1931 with 10° Standard Observer from 1964 and D65 source) was used for color analysis, represented as coordinates x, y and z. (see the SI for more details). A HazeGard Plus hazemeter apparatus from OAKLAND Inst. Corp., Shakopee, MN, USA was used to measure at once the haze, transmission and clarity values following the Standard Test Method 'ASTM D-1003'.

Table 2. Composition of the prepared cluster-PVP colloids.

Sample	$K_4[\{Nb_5TaX^i_{12}\}X^a_6]$ (g·L^{-1})*	PVP (%$_{wt}$)
$\{Nb_5TaX^i_{12}\}$-20	20	10%$_{wt}$
$\{Nb_5TaX^i_{12}\}$-16	16	10%$_{wt}$
$\{Nb_5TaX^i_{12}\}$-12	12	10%$_{wt}$
$\{Nb_5TaX^i_{12}\}$-8	8	10%$_{wt}$
$\{Nb_5TaX^i_{12}\}$-4	4	10%$_{wt}$
$\{Nb_5TaX^i_{12}\}$-2	2	10%$_{wt}$

* X = Cl, Br.

Electrospray ionization mass spectrometry (ESI-MS) measurements with ionization by electrospray or nanospray source were recorded on a quadrupole time-of-flight mass spectrometer (microtof-Q, Bruker-Daltonics, Bremen, Germany). The samples were analyzed both in negative and positive ion mode. Each solution sample was prepared to approximately 50 µmol·L^{-1} in either water or acetone. The water solutions were infused directly in an electrospray source using a syringe pump (flow rate 180 µL·h^{-1}), and the ESI process was assisted with a dry gas at 80°C. The acetone solutions were infused directly in a nanospray source with a dry gas at 55°C.

Raman scattering spectra were acquired on powders and thin films at room temperature using a LabRam high-resolution spectrometer coupled with a confocal microscope (Horiba Jobin Yvon, Edison, NJ, USA), 600 g/mm gratings and 10 × objective. A He-Ne 633 nm laser was used for scattering excitation. Raman spectra were recorded at room temperature with an exposure duration of 100 s and 2 accumulations. The calibration of the Raman spectrometer was performed using the main Raman band of silicon wafer (520 cm^{-1}). A soda-lime glass sample holder was used in all cases.

III. Results and discussion

3.1. Study of the powders and the colloidal solutions

The flexibility of homometallic octahedral niobium or tantalum cluster compounds in terms of composition and oxidation state, as well as their nanometric sizes and high solubility make them unique inorganic objects [40,41,45,46]. The chemical nature of the metallic cluster and the ligands to which it is bound as well as the VEC value make it possible to modulate the optical properties to absorb UV and NIR radiations [35–41]. It is then possible to modify these parameters to obtain one or more compositions in accordance with the desired application by mixing the metal in the metallic core or by changing the ligands. In order to modulate the optical properties of the cluster, new compositions of heterometallic clusters were developed in the past. It has clearly been shown that the spectroscopic properties of heterometallic clusters differ from a simple mixture of homometallic clusters [47,48].

Recently, M. Wilmet and C. Lebastard, clearly demonstrated by combining experimental and computational studies that the best optical properties for UV-NIR blockers are expected for the $K_4[\{Nb_{6-x}Ta_xX^i_{12}\}X^a_6]$ (X = Cl, Br; X = 1 and 2) cluster compounds compared to the corresponding homometallic ones [40,49,50]. The morphology and purity of the synthesized powders were confirmed by XRDP, FE-SEM and EDX analysis (Figures S1 and S2 and Tables S1 and S2). The full characterization of these compounds will be published separately. All data were consistent with previously published results on $[\{M_6X^i_{12}\}X^a_6]$ cluster units (M = Nb, Ta; X = Cl, Br) [47–50].

The Raman spectra of the $K_4[\{Nb_5TaX^i_{12}\}X^a_6]$ (X = Cl, Br) cluster compounds recorded at room temperature are given in Figure 2.

The experimental spectra of the two $K_4[\{Nb_5TaX^i_{12}\}X^a_6]$ powders exhibit similar characteristics to those of the $K_4[\{Nb_6X^i_{12}\}X^a_6]$ powders (Figure 2). The indexations of the peaks are given in Table S3. For the $[\{Nb_5TaCl^i_{12}\}Cl^a_2(H_2O)^a_4]\cdot 4\,H_2O$ aquo-complexes, to a first approximation, the bands are in good agreement with the spectrum reported for $[\{Nb_6Cl^i_{12}\}Cl^a_2(H_2O)^a_4]\cdot 4\,H_2O$ (Figure S4 and Table S3) [40,45].

Distilled water and acetone were selected as the dispersing media to obtain stable and transparent solutions. The optical absorption of the $K_4[\{Nb_5TaX^i_{12}\}X^a_6]$ (X = Cl, Br) cluster compounds and the $[\{Nb_5TaCl^i_{12}\}Cl^a_2(H_2O)^a_4]\cdot 4\,H_2O$ aquo-complex dispersed in water and acetone solvents are reported in Figures S5 and S6, respectively. For $K_4[\{Nb_5TaCl^i_{12}\}Cl^a_6]$, the main absorption peak in the UV region is located at 388 nm in water and 416 nm in acetone. In the NIR region, a large peak at 873 nm is observed for water (with a small shoulder at lower energy ≈650 nm), whereas acetone presents peaks at higher wavelengths, one at 993 nm and a large peak shoulder around 1300 nm. As already demonstrated for Ta_6 and Nb_6 clusters [45,50], this behavior clearly indicated the chemical instability of the reduced $\{Nb_5TaCl^i_{12}\}^{2+}$ cluster cores in acetone in the presence of oxygen and its oxidation into $\{Nb_5TaCl^i_{12}\}^{3+/4+}$ cluster cores (VEC = 14 or 15) during the dissolution process of $K_4[\{Nb_5TaCl^i_{12}\}Cl^a_6]$ in oxygenated acetone media. Similar results were obtained for $K_4[\{Nb_5TaBr^i_{12}\}$

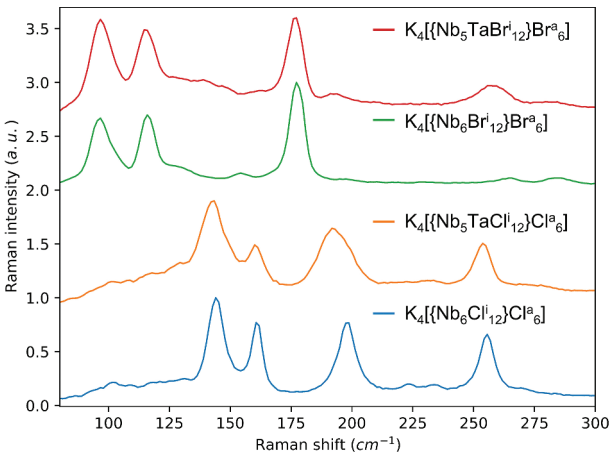

Figure 2. Raman spectra of $K_4[\{Nb_5TaX^i_{12}\}X^a_6]$. The homometallic spectra are added for comparison.

Br^a_6], nevertheless the optical properties are less interesting due to a stronger absorption in the visible range. Regarding the [{$Nb_5TaCl^i_{12}$}$Cl^a_2(H_2O)^a_4$]·4 H_2O aquo-complexes, after solubilization in water, the UV-Vis-NIR spectrum presents superimposable bands with the corresponding precursors K_4[{$Nb_5TaX^i_{12}$}X^a_6] (X = Cl, Br) cluster compounds dispersed in water, so it was inferred that the solutions contain the same species, i.e. [{$Nb_5TaX^i_{12}$}$(H_2O)^a_6$]$^{2+}$ cluster units with a VEC = 16 (Figure S5).

The mass spectra in both positive and negative modes in water and acetone are presented in Figures S7 and S8 and display series of $Nb_{6-x}Ta_x$ clusters ($0 \leq x \leq 4$) centered on the expected Nb_5Ta composition (× = 1). In water, only positive ions are detected: among the detected Nb_5Ta cluster ions, [$Nb_5TaX_{12}(H_2O)_6$]$^{2+}$ largely dominates, with a significant contribution of [$Nb_5TaX_{12}(H_2O)_5$]$^{2+}$ in the case of X = Br. These compositions correspond to clusters with a VEC = 16, which indicates that the complete substitution of the chlorine or bromine apical ligands by water molecules occurs in water media without oxidation, as already observed for [{$Ta_6Br^i_{12}$}Br^a_6]$^{4-}$ cluster units [45]. In acetone, only negative ions are detected. In the case of Nb_5Ta clusters, the ions have the composition [Nb_5TaX_{18}]$^{2-}$, i.e. no ligand substitution is observed in acetone. However, interestingly, this cluster composition corresponds to VEC = 14, which means that the cluster core is fully oxidized (likely by O_2 in an acetone). We assumed that these mass results confirm the other complementary results, especially the Raman and optical absorption. Indeed, the evolution of the optical absorption in water of the whole series from x = 0 to 6 confirmed without ambiguity the presence of the main targeted cluster in the solution [41].

Based on these results, water was selected as the best solvent for the preparation of the @PVP film nanocomposites. Indeed, the solubility of the cluster compounds is higher in the presence of water and the reduced formed (VEC = 16) is stabilized, which is required to optimize the values of T_L and T_E for solar glazing applications [49,50].

3.2. Study of the @PVP nanocomposite films

PVP is an inert, nontoxic, temperature-resistant, pH-stable, biodegradable and biocompatible polymer that has been widely used for a long time as excipients in pharmaceutical, food or cosmetic applications [51,52]. More recently, it was used as a solid polymer electrolyte in high energy rechargeable batteries, supercapacitors, fuel cells, photoelectrochemical and electrochromic displays [52–56], or as a matrix for tandem solar concentrators coating [57–60]. Previous works from our group reported the use of PVP for the preparation of functional nanocomposite thin films based on Mo_6, Nb_6 and Ta_6 metal atom cluster compounds (Table 1) [35,36,38,40,61,62].

For clarity, the detailed results obtained with K_4[{$Nb_5TaBr^i_{12}$}Br^a_6] cluster compounds are presented in the SI (Figures S9 and S10 and Table S4). The films, prepared by drop-casting, were first structurally and chemically analyzed to determine their homogeneity and uniformity. Optical and vibrational properties of the {$Nb_5TaX^i_{12}$}@PVP films were also characterized to evaluate the cluster core oxidation state and compared to the {$Nb_6Cl^i_{12}$}@PVP films [40,50].

Figure 3 shows the cross-sectional optical image of the film {$Nb_5TaCl^i_{12}$}-12@PVP and reveals a dense and homogeneous coating with an average thickness of 65 µm (±1 µm). The concentration of the nanoclusters has no impact on the thickness in the studied

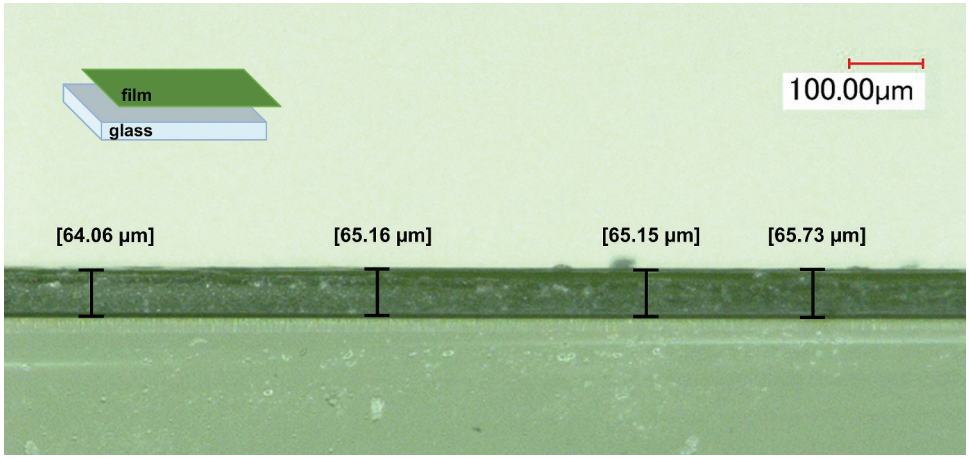

Figure 3. Example of digital microscope pictures of the cross section of a {$Nb_5TaCl^i_{12}$}-12@PVP nanocomposite film on glass substrate.

range, it is affected only by the molar mass and the concentration of PVP ($\%_{wtPVP}$) are the important parameters.

Figure 4 shows the UV-Vis-NIR spectra of the films with concentrations equal to 0, 2, 4, 8, 12, 16 and 20 $g{\cdot}L^{-1}$. The film without metal atom clusters (0 $g{\cdot}L^{-1}$) absorbs under 300 nm and is 86% transparent from 370 nm. As expected for the reference, this film is colorless (Figure S9, left), and at contrary, the film's absorption becomes stronger by increasing the concentration of clusters (Figures S9 right and S10 for the bromine cluster compounds). In Figures 4 and S10, the good transmission in the visible range for these nanocomposite films is attributed to the good dispersion in the polymer matrix, and the low absorption of the nanosized aquo-complexes, resulting in low scattering losses as suggested by Rayleigh theory. Indeed, vibrational frequencies of the $\{Nb_5TaCl^i_{12}\}$ cluster core in PVP are closer to those of the $\{Nb_6Cl^i_{12}\}$ cluster core in PVP (Figure S4) [40,50]. It was observed that as the cluster concentration of the deposition solution increased, so did the absorption intensity in the UV and NIR ranges. Moreover, the position of the NIR bands at maximum absorption does not change according to the concentration of the metal atom clusters, which confirms the VEC = 16 and the stability of the $[\{Nb_5TaX^i_{12}\}X^a_2(H_2O)^a_4]$ aquo-complexes (X = Cl, Br) in the PVP matrix.

The haze, clarity and S_{NIR} were measured for the film $\{Nb_5TaCl^i_{12}\}$-12.0@PVP. The very low haze (0.7%) and very high clarity (99.4%) values demonstrate the high potential of these nanocomposite coatings for application in window glass. Other important FOM values are presented in Table 3 (for $K_4[\{Nb_5TaBr^i_{12}\}Br^a_6]$ see SI Table S4) confirmed this point. The T_L and T_E decrease with the cluster concentration and conversely the T_L/T_E ratio increases, until reaching a limit of approximately 1.33 and a saturation (in transmission) in the NIR. When the concentration of the clusters ($\%_{wt}$ ≥20 $g{\cdot}L^{-1}$) continues to increase, the T_L value decreases under the accepted limit for window applications (50%), without the improvement of absorption in the NIR. This value of 1.33 is the best value obtained for coatings based on Ta_6 or Nb_6 metal atom clusters (Table 1). The S_{NIR} values increase with the concentration of nanoclusters and reach quite good values compared to other systems like Ga doped CuS nanocrystals nanocomposite films (range from 46.1% to 72.4%) [8]. Nevertheless, the S_{NIR} values are slightly depending on the thickness of the film, for instance, for the $\{Nb_5TaCl^i_{12}\}$-12.0@PVP films, the S_{NIR} values increase from 48.8% to 52.6% for a thickness of 65 µm and 85 µm, respectively, so it is difficult to compare.

In order to improve and to reach the best T_L/T_E and S_{NIR} values, the coating was directly deposited on ITO@glass instead of clear glass (Figure 5). Cluster units present a strong absorption between 760 nm and 1100 nm, whereas ITO has a reflective property regarding NIR radiation above 1400 nm. The use of ITO@glass as substrates is complementary to clusters for solar control and has a high impact in terms of T_E value (30.6% instead of 40.7%) with a large increase in the ratio of T_L/T_E. Thus, the preparation of a two-layer nanocomposite $\{Nb_5TaCl^i_{12}\}$-12@PVP@ITO@glass is clearly beneficial for the optical properties with a T_L/T_E ratio equal to 1.73 (T_L = 53%; T_E = 30.6%) and a S_{NIR} (78.3%), which are the best FOM values

Table 3. FOM values and CIE color coordinates for the chlorine nanocomposite films (thickness around 65 µm). Reproduced by permission from 41.

Cluster core-concentration	T_L	T_E	T_L/T_E	x	y	z	S_{NIR} (%)
$\{Nb_5TaCl^i_{12}\}$-20.0	47.1	35.6	1.32	0.38	0.45	0.17	57.8
$\{Nb_5TaCl^i_{12}\}$-16.0	54.1	40.7	1.33	0.37	0.43	0.20	54.4
$\{Nb_5TaCl^i_{12}\}$-12.0	62.9	48.3	1.30	0.35	0.41	0.24	48.8
$\{Nb_5TaCl^i_{12}\}$-8.0	68.8	54.5	1.26	0.34	0.39	0.26	43.7
$\{Nb_5TaCl^i_{12}\}$-4.0	79.6	68.3	1.16	0.33	0.36	0.30	31.1
$\{Nb_5TaCl^i_{12}\}$-2.0	85.1	77.6	1.10	0.32	0.35	0.33	22.2

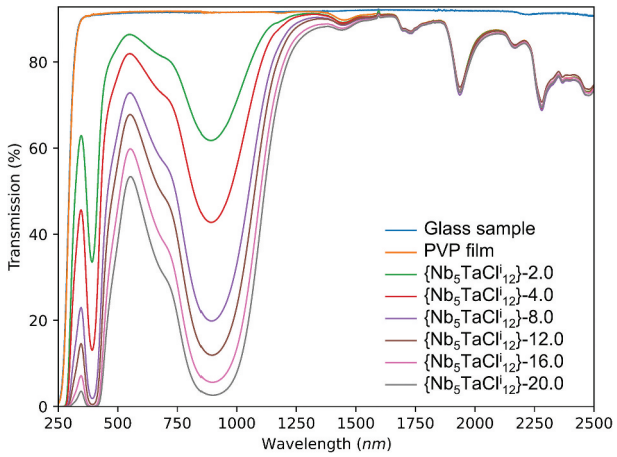

Figure 4. UV-Vis-NIR transmission spectra of the chlorine nanocomposite films for concentrations ranging from 0 to 20 $g{\cdot}L^{-1}$. Reproduced by permission from 41.

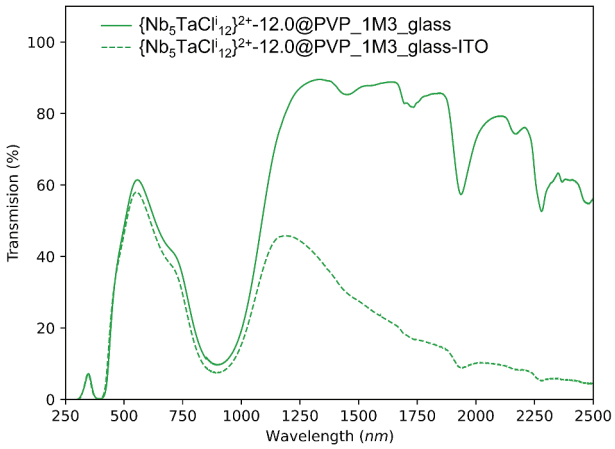

Figure 5. UV-Vis-NIR transmission spectra on glass and ITO@glass substrates for the $\{Nb_5TaCl^i_{12}\}$-12@PVP nanocomposite films.

obtained for nanocomposites based on octahedral metal atom clusters and some of the best for UV and NIR blocker nanocomposite coatings in the literature (shown in Table 1 and [8]). By comparison, an ideal window, corresponding to a visible transparent film (90% of transmittance between 400 and 780 nm) absorbing 100% of UV (200–400 nm) and NIR (780–2000) radiations, has a T_L/T_E ratio of 1.85. Thus, these values show significant improvement, 50% for the S_{NIR} value and around 30% comparing of the best T_L/T_E ratio of the $\{Nb_5TaCl^i_{12}\}$-12@PVP@glass nanocomposite ($T_L/T_E = 1.33$, this work) and 50% compared to commercial ITO@glass ($T_L/T_E = 1.15$, [36]).

In parallel, the CIE coordinates have been determined from the UV-Vis-NIR spectra of Figures 4 and S10. Fig. S11 shows the CIE chromaticity coordinates of all the films. These coordinates confirm the greenish color of the films. As expected, the evolution of these colors, as a function of the concentration of nanoclusters, is fairly linear as the composites kept the same VEC (VEC = 16). Indeed, the stability of the VEC versus temperature and pH is an important issue before a possible industrial use of these coatings. It is well-known that Nb_6 and Ta_6 based clusters compounds are not stable at very high pHs [63,64]. To demonstrate the stability of the deposition solutions, their pH values were adjusted to 2 with hydrochloric or oxalic acids, then the films obtained were dried at 50°C in air for 18 hours and compared with the film 'control' whose pH was not modified (Figure 6).

Progressive oxidation of the $\{Nb_5TaCl^i_{12}\}^{2+}$ cluster core incorporated into the matrix was observed, depending on the type of acid and the drying temperature. It was observed that the addition of hydrochloric acid greatly favors the oxidation of the cluster units, in particular, when the film is heated to 50°C. At room temperature, the addition of oxalic acid has no impact and the spectrum can be superimposed on that of the 'control' film. The addition of oxalic acid tends to reduce the oxidation of the cluster units during drying at 50°C compared to the 'control' film. As a reducing agent, oxalic acid makes it possible to slightly reduce the intensity of the absorption band beyond 1100 nm.

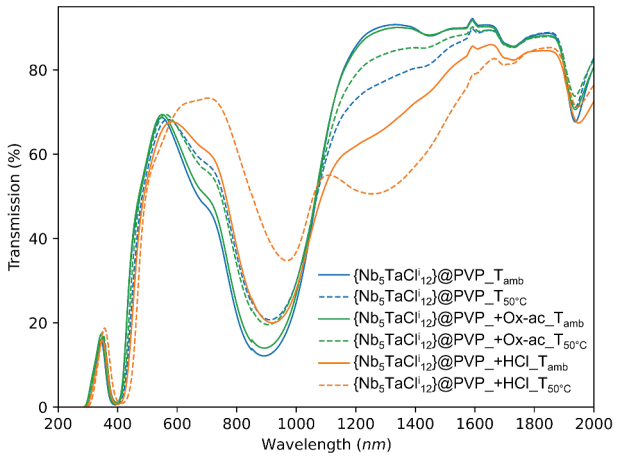

Figure 6. UV-Vis-NIR transmission spectra for the $\{Nb_5TaCl^i_{12}\}$-12@PVP nanocomposite films deposited on glass substrates and dried at room temperature or 50°C/18h by using different acid conditions.

Unlike hydrochloric acid, oxalic acid prevents oxidation of the clusters at room temperature. However, the use of oxalic acid does not fully control the optical properties of cluster patterns, especially when drying at elevated temperature. It is desirable to identify a better reducing agent, potentially complementary to oxalic acid, to overcome the oxidation of the clusters, even during moderate heat treatments (<100°C). The use of a $SnCl_2$ as a reducing agent has already been mentioned in the SI for the synthesis of aquo-complexes $[\{Nb_5TaCl^i_{12}\}Cl^a_2(H_2O)^a_4]\cdot 4\,H_2O$ requires the addition of a $SnCl_2$ to maintain the clusters at a VEC = 16 and thus compensate for the oxidizing conditions of the acid medium at 80°C. Indeed, the standard potential of the Sn^{4+}/Sn^{2+} couple is $E°Sn^{2+}/Sn = 0.15$ V vs. ECS and the addition of a tin salt in a @PVP solution should act in the same way. To prevent the oxidation of the clusters, an excess of $SnCl_2.2\,H_2O$ (m = 250 mg/g of $K_4[\{Nb_5TaCl^i_{12}\}Cl^a_6]$) is added directly to the previous process with the dissolution of $K_4[\{Nb_5TaX^i_{12}\}X^a_6]$ in the aqueous solution. Once the solvent was evaporated at room temperature and the film has been formed, the substrates are subjected to heat treatments, in order to study the impact of the tin salt on the evolution of the optical properties of the nanoclusters as a function of temperature (50°C, 80°C and 100°C during 18 h). Figure 7 displays the UV-Vis-NIR spectra of heat-treated films, prepared by the colloidal solutions containing $SnCl_2$, immediately after heat treatment (Figure 7, left), and after 1 year of storage under laboratory conditions (Figure 7, right). Photographs of the films are displayed in Figure 8. The UV-Vis spectra in transmission show no trace of oxidation of the cluster units. The clusters retain their degree of oxidation and VEC value of 16, despite the heat treatment, even after 1 year under ambient conditions of temperature, pressure and humidity. The use of such a reducing agent makes it possible, without any additional step, to avoid any change in the optical properties of the cluster units after heat treatments up to temperatures of at most 100°C.

IV. Conclusions

The work presented herein shows an original nanoarchitectonic strategy [65] to design the best cluster-based nanocomposite coatings with the optimized UV and NIR blocking properties of metal atom clusters. The colloids of $K_4[\{Nb_5TaX^i_{12}\}X^a_6]$ cluster

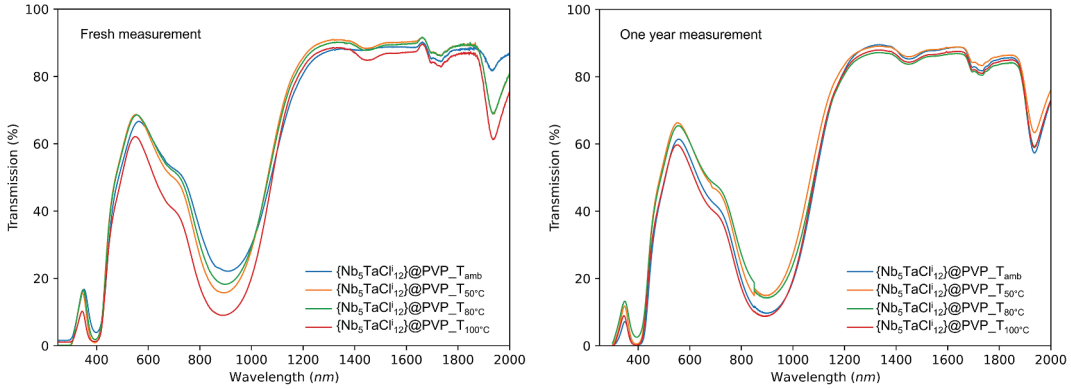

Figure 7. UV-Vis-NIR transmission spectra on glass substrates at room temperature or temperature ranging from 50°C to 100°C for the $\{Nb_5TaCl^i_{12}\}$-12@PVP nanocomposite films. Left: fresh measurements; right: measurement after 1-year aging at room temperature. Reproduced by permission from 41.

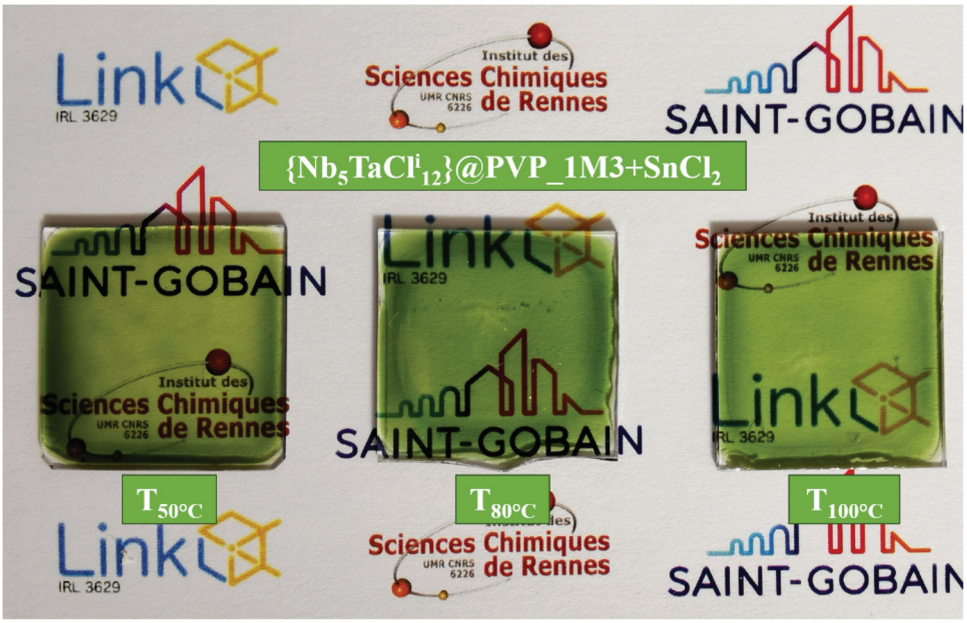

Figure 8. Picture of the nanocomposite films after 1-year aging for the $\{Nb_5TaCl^i_{12}\}$-12@PVP nanocomposite films.

compounds (X = Cl, Br) were prepared by a simple, low-cost, aqueous chemistry and then dispersed into a PVP matrix. The resulting solutions were used to fabricate highly visibly transparent and UV and NIR absorbent films by drop casting. The chloride-based cluster and aquo-complex compounds were identified as the best compromise compared to bromide ones. The UV and NIR absorption of such systems is strongly dependent on the concentration and the oxidation state of the metal cluster. The VEC has to be maintained at a value of 16 in order to keep the best UV-NIR absorption and the largest visible optical transmission, especially during moderate thermal treatment (100°C). This was made possible by adding a reducing agent, $SnCl_2$, directly into the water solution before the deposition of the film, without additional steps. This simple, low cost and low toxicity process preserved the optimal optical properties of the film up to 100°C and up to 1 year. A significant improvement of 30% in the T_L/T_E FOM was obtained compared to the previous results on nanocomposite coatings based on metal atom clusters. This new study demonstrated that metal atom cluster nanocomposites coated on ITO@glass, with an improved T_L/T_E and S_{NIR} FOM up to 1.73 and 78.3% respectively, are a very promising UV and NIR blocking pigments, which allow the filtering of the most energetic UV and NIR wavelengths.

Acknowledgement

A part of this work was supported by the Project CLIMATE ANR-17-CE09-0018. A part of this work was carried out in the France–Japan International Collaboration Framework ICGP NIMS-Université de Rennes 1 (UR1). C.L. thanks NIMS for his internship support in Japan under the ICGP agreement. The authors thank the CMEBA platform (Francis Gouttefangeas and Loic Joanny) from ScanMAT, UAR 2025 University of Rennes 1-CNRS for the FE-SEM

images and EDX analyses. The authors are very grateful to Bertrand Lefeuvre ISCR UMR6226 CNRS-UR1 and Alain Moréac from IPR UMR6252 CNRS-UR1 for the Raman investigations, which were performed using facilities available on SIR Plateforms from ScanMAT, UAR 2025 University of Rennes 1-CNRS. ScanMAT, received a financial support from the European Union through the European Regional Development Fund (ERDF), the Département d'Ille et Vilaine, Rennes Métropole and Région Bretagne (2015–2020 CPER project SCANMAT). The authors thank Dr C. Hassam at LINK for his precious advices and English polishing.

Disclosure statement

No potential conflict of interest was reported by the author(s).

Funding

The work was supported by the Agence Nationale de la Recherche [ANR-17-CE09-0018]; Centre National de la Recherche Scientifique [-]; National Institute for Materials Science [-]; Saint-Gobain [-]; Université de Rennes 1 [-].

ORCID

Clément Lebastard http://orcid.org/0000-0002-4302-3603
Stéphane Cordier http://orcid.org/0000-0003-0707-3774
Luke MacAleese http://orcid.org/0000-0001-8821-6049
Philippe Dugourd http://orcid.org/0000-0003-4395-1140
Naoki Ohashi http://orcid.org/0000-0002-4011-0031
Tetsuo Uchikoshi http://orcid.org/0000-0003-3847-4781
Fabien Grasset http://orcid.org/0000-0002-4911-0214

References

[1] Santamouris M. Energy in the urban built environment: the role of natural ventilation. Ghiaus C & Allard F, editors. Natural Ventilation in the Urban Environment: Assessment and Design. 2005:1–19; London: Earthscan. doi:10.4324/9781849772068
[2] IPCC. Climate change 2021: the physical science basis. 2021.
[3] Bastide A, Lauret P, Garde F, et al. Building energy efficiency and thermal comfort in tropical climates. Presentation of a numerical approach for predicting the percentage of well-ventilated living spaces in buildings using natural ventilation. Energy Build. 2006;38 (9):1093–1103. DOI:10.1016/j.enbuild.2005.12.005
[4] Granqvist CG. Solar energy material. Adv Mater. 2003;15(21):1789–1803.
[5] Smith GB, Deller CA, Swift PD, et al. Nanoparticle-Doped polymer foils for use in solar control glazing. J Nanopart Res. 2002;4(1/2):157–165. DOI:10.1023/A:1020186701109
[6] Zheng L, Xiong T, Shah KW. Transparent nanomaterial-based solar cool coatings: synthesis, morphologies and application. Sol Energy. 2019;193:837–858.
[7] Greenberg CB. Enabling thin films for solar control transparencies: a review. J Electrochem Soc. 1993;140 (11):3332.
[8] Gao Q, Wu X, Huang T. Greatly improved NIR shielding performance of CuS nanocrystals by gallium doping for energy efficient window. Ceram Int. 2021;47(17):23827–23833.
[9] Schelm S, Smith GB, Garrett PD, et al. Tuning the surface-plasmon resonance in nanoparticles for glazing applications. J Appl Phys. 2005;97(12):124314. DOI:10.1063/1.1924873
[10] Stokes NL, Edgar JA, McDonagh AM, et al. Spectrally selective coatings of gold nanorods on architectural glass. J Nanopart Res. 2010;12(8):2821–2830. DOI:10.1007/s11051-010-9864-y
[11] Xu X, Gibbons TH, Cortie MB. Spectrally-Selective gold nanorod coatings for window glass. Gold Bull. 2006;39(4):156–165.
[12] Chen W, Thoreson MD, Ishii S, et al. Ultra-Thin ultra-smooth and low-loss silver films on a germanium wetting layer. Opt Express. 2010;18 (5):5124–5134. DOI:10.1364/OE.18.005124
[13] Chew C, Bishop P, Salcianu C, et al. Aerosol-Assisted deposition of gold nanoparticle-tin dioxide composite films. RSC Adv. 2014;4(25):13182–13190. DOI:10.1039/C3RA46828C
[14] Carboni M, Carravetta M, Zhang XL, et al. Efficient NIR light blockage with matrix embedded silver nanoprism thin films for energy saving window coating. J Mater Chem C. 2016;4(8):1584–1588. DOI:10.1039/C6TC00026F
[15] Sousa-Castillo A, Ameneiro-Prieto O, Comesaña-Hermo M, et al. Hybrid plasmonic nanoresonators as efficient solar heat shields. Nano Energy. 2017;37:118–125.
[16] Besteiro LV, Kong XT, Wang Z, et al. Plasmonic glasses and films based on alternative inexpensive materials for blocking infrared radiation. Nano Lett. 2018;18 (5):3147–3156. DOI:10.1021/acs.nanolett.8b00764
[17] Granqvist CG. Electrochromic tungsten oxide films: review of progress 1993–1998. Sol Energy Mater Sol Cells. 2000;60(3):201–262.
[18] Kang L, Gao Y, Luo H, et al. Nanoporous thermochromic VO $_2$ films with low optical constants, enhanced luminous transmittance and thermochromic properties. ACS Appl Mater Interfaces. 2011;3 (2):135–138. DOI:10.1021/am1011172
[19] Zheng H, Ou JZ, Strano MS, et al. Nanostructured tungsten oxide – properties, synthesis, and applications. Adv Funct Mater. 2011;21(12):2175–2196. DOI:10.1002/adfm.201002477
[20] Guo C, Yin S, Huang L, et al. Discovery of an excellent IR absorbent with a broad working waveband: Cs_xWO_3 nanorods. Chem Commun. 2011;47 (31):8853–8855. DOI:10.1039/c1cc12711j
[21] Koebel MM, Nadargi DY, Jimenez-Cadena G, et al. Transparent, conducting ATO thin films by epoxide-initiated sol–gel chemistry: a highly versatile route to mixed-metal oxide films. ACS Appl Mater Interfaces. 2012;4(5):2464–2473. DOI:10.1021/am300143z
[22] Gao Y, Wang S, Luo H, et al. Enhanced chemical stability of VO_2 nanoparticles by the formation of SiO_2/VO_2 core/shell structures and the application to transparent and flexible VO_2-based composite

foils with excellent thermochromic properties for solar heat control. Energy Environ Sci. 2012;5 (3):6104–6110. DOI:10.1039/c2ee02803d
[23] Llordés A, Garcia G, Gazquez J, et al. Tunable near-infrared and visible-light transmittance in nanocrystal-in-glass composites. Nature. 2013;500 (7462):323–326. DOI:10.1038/nature12398
[24] Garcia G, Buonsanti R, Llordes A, et al. Near-Infrared spectrally selective plasmonic electrochromic thin films. Adv Opt Mater. 2013;1(3):215–220. DOI:10.1002/adom.201200051
[25] Trenque I, Mornet S, Duguet E, et al. Encapsulation of ZnO particles by metal fluorides: towards an application as transparent insulating coatings for windows. Opt Mater. 2013;35(3):661–667. DOI:10.1016/j.optmat.2012.10.056
[26] Soumya S, P MA, Paul L, et al. Near IR reflectance characteristics of PMMA/ZnO nanocomposites for solar thermal control interface films. Sol Energy Mater Sol Cells. 2014;125:102–112.
[27] Kang L, Xu W, Wang K, et al. Transparent $(NH_4)_x WO_3$ colloidal dispersion and solar control foils: low temperature synthesis, oxygen deficiency regulation and NIR shielding ability. Sol Energy Mater Sol Cells. 2014;128:184–189.
[28] Li Y, Liu J, Liang J, et al. Tunable solar-heat shielding property of transparent films based on mesoporous Sb-Doped SnO_2 microspheres. ACS Appl Mater Interfaces. 2015;7(12):6574–6583. DOI:10.1021/am508711p
[29] Gao Q, Wu X, Cai L. Dual functionality of $K_{0.3}WO_3/Ag_2O$ nanocomposites for smart window: energy saving and visible photocatalytic self-cleaning performance. Sol Energy Mater Sol Cells. 2019;196:111–118.
[30] Chao L, Bao L, Wei W, et al. A review of recent advances in synthesis, characterization and NIR shielding property of nanocrystalline rare-earth hexaborides and tungsten bronzes. Sol Energy. 2019;190:10–27.
[31] Yao Y, Chen Z, Wei W, et al. $Cs_{0.32}WO_3$/PMMA nanocomposite via in-situ polymerization for energy saving windows. Sol Energy Mater Sol Cells. 2020;215. 110656.
[32] Shao J, Shen H, Gao K, et al. UV- and NIR-blocking properties of ZnO/ATO bilayer films prepared by RF magnetron sputtering. Opt Mater. 2021;118:111287.
[33] Shen B, Wang Y, Lu L, et al. Enhanced spectral modulation of $CsWO_3$ nanocrystals through anionic doping for energy-efficient glazing. Sol Energy Mater Sol Cells. 2022;236:111519.
[34] Takeda H, Kuno H, Adachi K. Solar control dispersions and coatings with rare-earth hexaboride nanoparticles. J Am Ceram Soc. 2008;91:2897–2902.
[35] Renaud A, Wilmet M, Truong TG, et al. Transparent tantalum cluster-based UV and IR blocking electrochromic devices. J Mater Chem C. 2017;5 (32):8160–8168. DOI:10.1039/C7TC01964E
[36] Nguyen TKN, Renaud A, Wilmet M, et al. New ultra-violet and near-infrared blocking filters for energy saving applications: fabrication of tantalum metal atom cluster-based nanocomposite thin films by electrophoretic deposition. J Mater Chem C. 2017;5(40):10477–10484. DOI:10.1039/C7TC02454A
[37] Chen W, Wilmet M, Truong TG, et al. Embedding hexanuclear tantalum bromide cluster $\{Ta_6Br_{12}\}$ into SiO_2 nanoparticles by reverse microemulsion method. Heliyon. 2018;4(6):4e00654. DOI:10.1016/j.heliyon.2018.e00654
[38] Nguyen TKN, Dubernet M, Matsui Y, et al. Transparent functional nanocomposite films based on octahedral metal clusters: synthesis by electrophoretic deposition process and characterization. R Soc Open Sci. 2019;6(3):181647. DOI:10.1098/rsos.181647
[39] Chen W, Nguyen TKN, Wilmet M, et al. ITO@SiO_2 and ITO@$\{M_6Br_{12}\}$@SiO_2 (M = Nb, Ta) nanocomposite films for ultraviolet-near infrared shielding. Nanoscale Adv. 2019;1:3693–3698.
[40] Lebastard C, Wilmet W, Cordier S, et al. Nanoarchitectonics of glass coatings for near-infrared shielding: from solid-state cluster-based niobium chlorides to the shaping of nanocomposite films. ACS Appl Mater Interfaces. 2022;14(18):21116–21130. DOI:10.1021/acsami.2c00308
[41] Lebastard C, Wilmet M, Cordier S, et al. Controlling the Deposition Process of Nanoarchitectonic Nanocomposites Based on {nb6–xtaxxi12}n+ Octahedral Cluster-Based Building Blocks (Xi = Cl, Br; $0 \le x \le 6$, n = 2, 3, 4) for UV-NIR blockers coating applications. Nanomaterials. 2022;12(12):2052. DOI:10.3390/nano12122052
[42] Eisenbraun R, Schafer H. Drei wege zur oxydation von $[Ta_6Cl_{12}]^{2+}$ ($[Ta_6Br_{12}]_2$+ und $[Nb_6Cl_{12}]^{2+}$) Z. Anorg Allg Chem. 1985;530(11):222–226.
[43] Parsons JA, Vongvusharintra A, Koknat FW. High temperature conproportionation of niobium pentahalide and niobium metal; a convenient route to hydrated cluster halides $Nb_6Cl_{14}{\cdot}8H_2O$ and $Nb_6Br_{14}{\cdot}8H_2O$. Inorg Nucl Chem Lett. 1972;8 (3):281–286.
[44] Koknat FW, Parsons JA, Vongvusharintra A. Metal cluster halide complexes. I. Efficient synthesis of hydrated hexanuclear niobium and tantalum cluster halides $M_6X_{14}.8H_2O$. Inorg Chem. 1974;13 (7):1699–1702.
[45] Wilmet M, Lebastard C, Sciortino F, et al. Revisiting properties of edge-bridged bromide tantalum clusters in the solid-state, in solution and vice versa : an intertwined experimental and modelling approach. Dalton Trans. 2021;50(23):8002–8016. DOI:10.1039/D0DT04200E
[46] Robin MB, Na K. Color and nonintegral valence in niobium and tantalum subhalides. Inorg Chem. 1965;4(7):978–984.
[47] Schäfer H, Spreckelmeyer B. Die verbindung $Nb_6Cl_{16}{\cdot}3C_2H_5OH$. J Less-Common Met. 1966;11:74–75.
[48] Preetz W, Harder K. Trennung und charakterisierung der metallgemischten cluster $[(Nb_nTa_{6-n})Cl^i_{12}]^{2+}$, n = 0-6. Z. Anorg Allg Chem. 1991;597:163–172. DOI:10.1002/zaac.19915970119
[49] Wilmet M. Thesis Rennes 1 Univ. 2018. Available from: http://www.theses.fr/2018REN1S108
[50] Lebastard C. Thesis Rennes 1 Univ. 2021. in press. Available from: http://www.theses.fr/s211547
[51] Kurakula M, Koteswara Rao GSN. Pharmaceutical assessment of polyvinylpyrrolidone (PVP): as excipient from conventional to controlled delivery systems with a spotlight on COVID-19 inhibition. J Drug Deliv Sci Technol. 2020;60:102046–102069.
[52] Younes M, Aquilina G, Castle L, et al. Re-Evaluation of polyvinylpyrrolidone (E 1201) and polyvinylpolypyrrolidone (E 1202) as food additives and extension of use of polyvinylpyrrolidone (E 1201. EFSA J. 2020;18(8):e06215.

[53] Aslan M, Weingarth D, Jäckel N, et al. Polyvinylpyrrolidone/polyvinyl butyral composite as a stable binder for castable supercapacitor electrodes in aqueous electrolytes. J Power Sources. 2014;266:374–383.
[54] Selvam S, Balamuralitharan B, N KS, et al. Novel high-temperature supercapacitor combined dye sensitized solar cell from a sulfated β-cyclodextrin/pvp/mnco $_3$ composite. J Mater Chem A. 2015;3(19):10225–10232. DOI:10.1039/C5TA01792K
[55] Kotok V, Vadym K. A Study of the influence of polyvinyl pyrrolidone concentration in the deposition electrolyte on the properties of electrochromic $Ni(OH)_2$ films. East-Eur J Enterp Technol. 2020;4/6(106):31–37.
[56] Kozlov DA, Shcherbakov AB, Kozlova TO, et al. Photochromic and photocatalytic properties of ultra-small PVP-stabilized WO_3 nanoparticles. Molecules. 2019;25(1):154–170. DOI:10.3390/molecules25010154
[57] Wu K, Li H, Klimov VI. Tandem luminescent solar concentrators based on engineered quantum dots. Nat Photonics. 2018;12(2):105–110.
[58] Zha H, Liu G, Han G. High-Performance laminated luminescent solar concentrators based on colloidal carbon quantum dots. Nanoscale Adv. 2019;1(12):4888–4894.
[59] Li Y, Zhang X, Zhang Y, et al. Review on the role of polymers in luminescent solar concentrators. J Polym Sci a Polym Chem. 2019;57(3):201–215. DOI:10.1002/pola.29192
[60] Kim A, Hosseinmardi A, Annamalai PK, et al. Review on colloidal quantum dots luminescent solar concentrators. ChemistrySelect. 2021;6(20):4948–4967. DOI:10.1002/slct.202100674
[61] Aubert T, Nerambourg N, Saito N, et al. Tunable visible emission of luminescent hybrid nanoparticles incorporating two complementary luminophores: ZnO nanocrystals and [Mo 6 Br 14] 2− nanosized cluster units. Part Part Syst Charact. 2013;30(1):90–95. DOI:10.1002/ppsc.201200047
[62] Truong TG, Dierre B, Grasset F, et al. Visible tunable lighting system based on polymer composites embedding ZnO and metallic clusters: from colloids to thin films. Sci Technol Adv Mater. 2016;17(1):443–453. DOI:10.1080/14686996.2016.1202724
[63] Allen RJ, Sheldon JC. Some studies of $Nb_6Cl_{14},7H_2O$ and analogous compounds. Aust J Chem. 1965;18(3):277–283.
[64] Hughes BG, Meyer JL, Fleming PB, et al. Chemistry of polynuclear metal halides. III Synthesis of some Niobium and Tantalum $M_6X_{12}^{n+}$ cluster derivatives. Inorg Chem. 1970;9(6):1343–1346. DOI:10.1021/ic50088a010
[65] Ariga K, Nishikawa M, Mori T, et al. Self-Assembly as a key player for materials nanoarchitectonics. Sci Technol Adv Mater. 2019;20(1):51–95. DOI:10.1080/14686996.2018.1553108